Exciton Diffusion and Interfacial Charge Separation in *meso*-Tetraphenylporphyrin/TiO_2 Bilayers: Effect of Ethyl Substituents

Annemarie Huijser,[†] Tom J. Savenije,[†] Jessica E. Kroeze,[‡] and Laurens D. A. Siebbeles*,[†]

Opto-Electronic Materials Section, Delft Research Centre for Sustainable Energy, DelftChemTech, Delft University of Technology, Mekelweg 15, 2629 JB, Delft, The Netherlands, and Centre for Electronic Materials and Devices, Imperial College London, London SW7 2AY, United Kingdom

Received: June 17, 2005; In Final Form: August 12, 2005

The photoinduced charge separation efficiency in porphyrin/TiO_2 bilayers has been determined using the time-resolved microwave conductivity (TRMC) technique. Porphyrins investigated are unsubstituted *meso*-tetraphenylporphyrin (TPP) and *meso*-tetra(4-ethylphenyl)porphyrin (TEPP). TEPP/TiO_2 bilayers exhibit a charge separation efficiency per incident photon at the Soret band maximum of 6.2%, which is considerably higher than the efficiency of 1.2% found for TPP/TiO_2 bilayers. Exciton diffusion lengths of 7 Å for TPP and 75 Å for TEPP are obtained from fitting a model for the charge separation efficiency to the experimental data. Optical measurements on the porphyrin derivatives on quartz yield a 20 times higher fluorescence quantum yield and a 7 times higher fluorescence rate constant for TEPP layers as compared to TPP layers. The exciton lifetime of 800 ps found for TEPP layers is considerably longer than the lifetime of 260 ps in TPP layers. The exciton diffusion coefficients, determined from the exciton diffusion length and the exciton lifetime, are found to be $2\cdot10^{-9}$ m^2/s for TPP and $7\cdot10^{-8}$ m^2/s for TEPP. The difference is discussed in terms of the presence of face-to-face dimers or larger aggregates in TPP layers.

Introduction

Solar cells consisting of a light-absorbing organic dye and an electron-accepting inorganic semiconductor exhibit advantages over silicon-based solar cells, including opportunities of cheap processing, chromatic flexibility, and a practically unlimited choice of materials.[1] The working principle of a dye-sensitized solar cell is based on the photophysical processes that are schematically depicted in Figure 1. The wide band gap semiconductor such as TiO_2 and SnO_2 does not absorb visible light, but is photosensitized by the dye layer. This dye layer absorbs photons from the visible part of the solar spectrum, thereby promoting an electron from the ground state to a higher energetic level (Figure 1, process 1). The resulting strongly bound electron−hole pair, which consists of the excited electron and a positively charged electron vacancy, is referred to as an exciton. These excitons may migrate to the interface with the semiconductor (3), where charge separation (CS) can occur by electron injection from the S_1 level of the dye layer into the conduction band of the semiconductor (7). Other competing processes are intersystem crossing to the triplet level (4) and decay to the ground state by radiationless decay (5) or under emission of a photon (6). The electrons and holes formed at the interface by charge separation can either recombine (8) or escape from each other. In a photovoltaic device, charges are collected by electrodes on top of the semiconductor film and the dye layer and can perform work in an external circuit.

The performance of flat organic/inorganic bilayer solar cells is typically much less than 1%.[2,3] The low performance is to a large extent due to the fact that the exciton diffusion length is small compared to the optical absorption length. For organic dyes, the light absorption length is typically 100 nm. However, the exciton diffusion length

$$\Lambda_E = \sqrt{D_E \tau_E} \qquad (1)$$

with D_E the exciton diffusion coefficient and τ_E the natural exciton lifetime is often found to be only a few nanometers.[4,5]

Because of this short exciton diffusion length, the photoactive part of the dye layer is restricted to a few monolayers near the interface. Excitons formed further away from the interface decay by nonradiative (5) or radiative (6) processes before reaching the interface and do not contribute to the photocurrent.

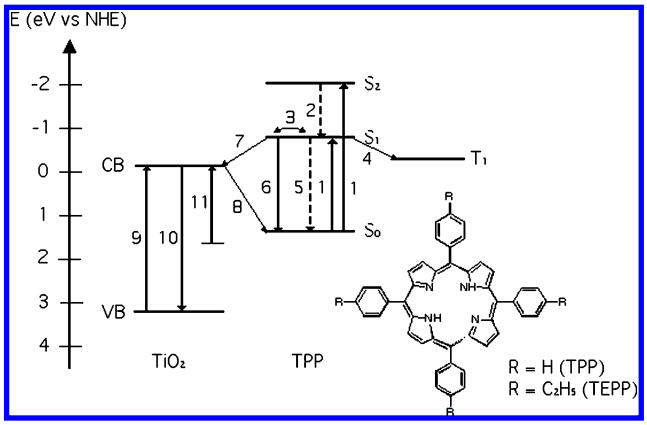

Figure 1. The energy levels of *meso*-tetraphenylporphyrin (TPP) in solution, the conduction (CB) and valence band (VB) positions of anatase TiO_2, and the processes occurring on optical excitation. The inset shows the chemical structure of the porphyrins investigated. Key: 1, photoexcitation; 2, internal conversion; 3, exciton diffusion; 4, intersystem crossing; 5, radiationless decay; 6, fluorescence; 7, interfacial electron transfer; 8, interfacial charge recombination; 9, direct band gap excitation; 10, intrinsic charge recombination; 11, sub-band gap excitation.

* L.D.A.Siebbeles@tnw.tudelft.nl.
[†] Delft University of Technology.
[‡] Imperial College London.

10.1021/jp053265e CCC: $30.25
Published on Web 10/07/2005

One way to overcome this problem is the use of nanocrystalline semiconductor films.[1,6,7] This results in a much larger interfacial area between the light-absorbing molecules and the semiconductor, thus reducing the mean distance excitons have to diffuse to reach the interface. A performance of more than 10% has been achieved for a cell based on an interpenetrating network of dye-coated nanocrystalline TiO_2 particles and a hole-transporting electrolyte.[6] However, because of complications involved in the use of a liquid electrolyte,[8] there is currently a great interest in the development of total solid-state organic/inorganic solar cells. For all solid-state nanocrystalline organic/inorganic solar cells, a maximum performance of 3−4% has been realized so far.[9−11]

An alternative approach to overcome the limited exciton diffusion length in organic dye layers involves enhancement of the exciton diffusion length within the dye layer. As follows from eq 1, this can be realized by enhancing the natural exciton lifetime and/or the exciton diffusion coefficient.

Porphyrin-based dyes have attracted considerable attention to be applied as sensitizers because of the overlap of their optical absorption spectrum with the solar emission spectrum. In combination with TiO_2 or SnO_2 as an electron acceptor, efficient charge separation has been observed.[12−18] Current research is focused on improvement of the interfacial electron injection yield by the use of binding groups and linkers,[19−24] on enhancement of the exciton diffusion length,[4,5,25−28] and on improvement of the charge transport properties.[23,29,30]

It is well-known that derivatives of tetraphenylporphyrins can form dimers or larger aggregates in solution[31−33] and in thin films.[32,34] Previous studies have shown that aggregation affects the exciton natural lifetime[33,35,36] and the quantum yield for interfacial electron injection (ϕ_{inj}).[37]

Recently, we have studied charge separation in *meso*-tetra(4-*n*-octylphenyl)porphyrin/TiO_2 bilayers.[25] The incident photon to charge separation efficiency (IPCSE) at the absorption maximum was found to be 10%. After heating above the crystalline−lamellar discotic phase transition temperature of the porphyrin, the IPCSE decreases to 1%. The change of the IPCSE has been attributed to a change of the porphyrin layer structure from isotropic before heating to an anisotropic layer consisting of columnar aggregates oriented with their long axes parallel to the TiO_2 substrate after heating. This negative temperature effect on the IPCSE is of course undesirable for practical use of porphyrin dyes in photovoltaic devices.

Also, the introduction of a Pd atom in *meso*-tetra(4-carboxyphenyl)porphyrin molecules has been found to increase the IPCSE at the absorption maximum from 1% to 12%.[38,39] Exciton transport in these porphyrin films occurs via the triplet level. The exciton diffusion length in these layers equals 28 nm, resulting from an exciton lifetime of 10 μs and an exciton diffusion coefficient of $8 \cdot 10^{-11}$ m^2/s. Exciton transport via the triplet route, however, is less attractive as compared to transport via the singlet route because of unwanted chemical degradation of the dye.[40,41]

The aim of the present work is to provide information on the exciton diffusion length and the efficiency of photoinduced charge separation in bilayers of the porphyrin derivatives *meso*-tetraphenylporphyrin (TPP) and *meso*-tetra(4-ethylphenyl)porphyrin (TEPP) with TiO_2. These porphyrins differ by an ethyl group at the *para*-phenyl positions (see inset of Figure 1). Steady-state optical absorption and fluorescence spectroscopy as well as fluorescence lifetime measurements on films spin-coated on quartz substrates were used to characterize the porphyrin layer. Charge separation efficiencies in porphyrin/TiO_2 bilayers were determined with the time-resolved microwave conductivity (TRMC) method. Excitons were created in the dye layer by illumination with a nanosecond laser pulse, which results in a change in conductivity due to electron injection into the TiO_2 film. Charge separation efficiencies were determined as a function of intensity, wavelength, and porphyrin layer thickness. Values for the exciton diffusion length and the interfacial injection yield were obtained by fitting an analytical model for exciton diffusion to the experimental data. Together with the measured fluorescence lifetimes, these values were used to derive the exciton diffusion coefficients in the porphyrin layers. The knowledge about the factors determining the exciton diffusion length is useful for the development of more efficient solar cells based on porphyrins.

Experimental Methods

Sample Preparation. Thin smooth TiO_2 films were purchased from Everest Coatings, Delft, The Netherlands. They were prepared by chemical vapor deposition onto $1 \times 12 \times 25$ mm^3 quartz substrates, followed by annealing in air at 450 °C for 1 h in order to obtain anatase TiO_2.[42] The TiO_2 film thickness was ca. 100 nm. *Meso*-tetraphenylporphyrin (TPP) and *meso*-tetra(4-ethylphenyl)porphyrin (TEPP) were purchased from Porphyrin Systems and Frontier Scientific, respectively, and were used without further purification. Thin porphyrin films were prepared by spin-coating from a solution in $CHCl_3$ (Anhydrous, 99+%, Aldrich) at 2500 rpm under N_2 atmosphere onto either a quartz or a TiO_2 substrate. Prior to film deposition, these substrates were dried at 450 °C for 1 h in order to remove H_2O from the surface. Film thicknesses of the porphyrin layers were determined by a Veeco Dektak 8 Stylus Profiler. The S_0 levels of TPP and TEPP were determined by cyclic voltammetry, using an Ag/AgCl reference electrode and a 0.5 M tetrabutylammonium perchlorate solution in acetonitrile. The position of the S_0 level was found to be equal to 1.3 eV vs normal hydrogen electrode (NHE) for both compounds.

Optical Characterization. Optical transmission spectra of dilute solutions of the porphyrin molecules in $CHCl_3$ were recorded with a Perkin-Elmer Lambda 40 UV−vis spectrometer. Optical transmission and reflection spectra of thin films were recorded with a Perkin-Elmer Lambda 900 UV/VIS/NIR spectrometer, using an integrating sphere. From the transmission and reflection spectra, the fraction of absorbed light (F_A) and the optical density (OD) were calculated.[17] Steady-state fluorescence spectra were recorded with a Photon Technology International photoluminescence setup.

Fluorescence lifetime measurements on dilute solutions were performed by illumination with a pulsed Megaplus N_2 laser (337 nm, pulse width < 1 ns) and detecting the fluorescence at 660 nm. Transient fluorescence data of thin films were collected using an IBH NanoLED-07 pulsed laser diode excitation source (404 nm, pulse width < 100 ps). The emission was detected through a 650 nm band-pass filter by a Hamamatsu microchannel plate photomultiplier. The total instrument response time was 100 ps. The resulting decay curves were analyzed using IBH DAS6 analysis software.

TRMC Measurements. The TRMC technique has been fully described previously.[5,43] The porphyrin/TiO_2 bilayers were mounted in an X-band microwave cavity at a position of maximum electric field. To exclude any O_2-induced degradation effects of the organic layer, sample preparation and experiments were performed under N_2 atmosphere. The microwave frequency used in these experiments was ca. 8.45 GHz.

Pulses in a wavelength range of 410 nm to 700 nm (pulse width 3 ns) were obtained by pumping an optical parametric oscillator (OPO) with the third harmonic of a Q-switched Nd:YAG laser (Infinity, Coherent). To obtain pulses with a wavelength in the UV part of the spectrum, visible laser pulses were frequency doubled by a single harmonic generator (SHG) yielding pulses with a width of 2.5 ns. The sample was illuminated either through the quartz substrate ("backside", BS) or through the porphyrin layer ("front-side", FS). The incident intensity was varied between $10^{11}-10^{13}$ photons/cm^2 per pulse, using metallic neutral density filters.

The formation of mobile charge carriers due to pulsed illumination leads to an increase of the conductance (ΔG), which is followed by an eventual decrease resulting from the decay of charge carriers. The change in microwave power reflected by the microwave measuring cell on pulsed illumination (ΔP) was monitored using microwave circuitry and detection equipment, which has been described previously.[43] The temporal change in reflected microwave power is related to ΔG by

$$\frac{\Delta P(t)}{P} = -K\Delta G(t) \tag{2}$$

The sensitivity factor K was determined as described previously[44] and had a value of $7\cdot10^4$ S^{-1} for the current cell design and materials. The change in conductance is related to the product of the average concentrations (N_i) and mobilities (μ_i) of charge carriers by

$$\Delta G(t) = e\beta L \sum N_i(t)\mu_i \tag{3}$$

In eq 3, β is the ratio between the broad and narrow inner dimensions of the waveguide (2.08 for the X-band waveguide used), L is the thickness of the TiO_2 layer, and e the elementary charge. From the maximum of the photoconductance over time (ΔG_{max}), the parameter $\eta\Sigma\mu$ is calculated according to

$$\eta\sum\mu = \frac{\Delta G_{max}}{e\beta I_0} \tag{4}$$

where I_0 is the integrated incident light intensity (photons/cm^2/pulse), $\Sigma\mu$ is the sum of the hole and electron mobilities, and η is the number of charge carrier pairs produced per incident photon at the time where the photoconductance is maximal.

For a bilayer system, the incident photon to charge separation efficiency (IPCSE) was derived in the following way. Since the electron mobility (μ_e) in anatase TiO_2 is much higher than the hole mobility, $\Sigma\mu$ is close to equal to the electron mobility.[45] The electron mobility in TiO_2 was obtained on direct band gap excitation (Figure 1, process 9) using UV (300 nm) radiation. At 300 nm, photons absorbed by the semiconductor lead to formation of free electrons in the conduction band, and hence

$$\sum\mu \approx \mu_e \approx \frac{[\eta\sum\mu]_{300nm}}{\phi F_{A,300nm}} \tag{5}$$

where ϕ is the quantum yield for charge carrier formation, which is assumed to be equal to 1.[46] In a porphyrin/TiO_2 bilayer, the mobility of holes in the porphyrin layer is much lower than the electron mobility in TiO_2;[45,47] therefore, only the production of mobile electrons in TiO_2 results in a measurable change of the microwave conductivity. From μ_e and $\eta\Sigma\mu$ obtained on pulsed illumination of a bilayer system with visible light, the IPCSE can thus be calculated using eq 6

$$\text{IPCSE} = \frac{[\eta\sum\mu]}{\mu_e}\cdot 100\ \% \tag{6}$$

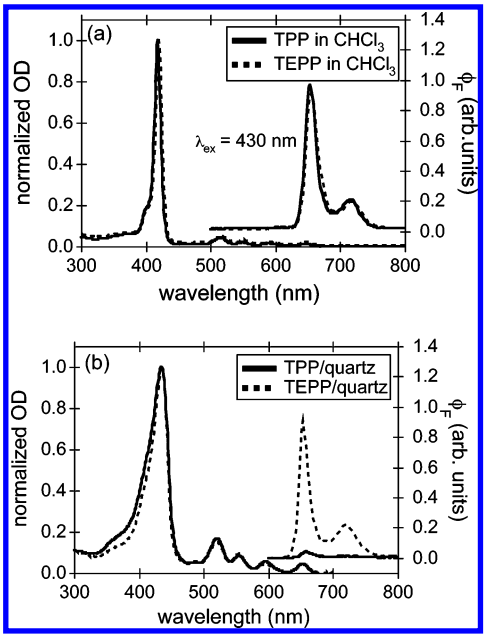

Figure 2. Normalized optical density spectra and relative fluorescence quantum yields as a function of wavelength for TPP (solid lines) and TEPP (dashed lines) in solution (a) and as spin-coated films (30 ± 5 nm) on quartz (b).

Results

Optical Characterization. Effects of chemical structure and intermolecular interactions on the photophysical properties of the materials were studied by absorption and fluorescence measurements on solutions and thin films. Figure 2a shows the normalized optical density spectra of dilute solutions of TPP and TEPP in $CHCl_3$, together with their steady-state fluorescence spectra. For both solutions, identical absorption and fluorescence spectra and fluorescence quantum yields were found. The S_0-S_2 transition results in a strong absorption band between 400 and 450 nm (the "Soret" band) with an absorption maximum at 420 nm. Transitions from S_0 to two energetically slightly different S_1 levels and their higher vibrational modes cause the less intense Q-bands between 500 and 700 nm.[48] From the observation that excitation at 430 nm and at 520 nm yield identical fluorescence spectra, it is concluded that electrons excited to the S_2 or a higher level decay rapidly to the S_1 level by internal conversion (Figure 1, process 2). The most intense fluorescence was recorded at 654 nm, which is due to the S_1-S_0 transition. The second fluorescence band at 716 nm is caused by a transition to a vibrationally excited state of the S_0 level.

Figure 2b shows the normalized optical density and fluorescence spectra of TPP and TEPP films on quartz. The absorption spectra of both films show a red shift and a broadening of the Soret band as compared to the spectra in solution. Both films exhibit a maximum absorption at 435 nm. In comparison to TEPP, the TPP film exhibits a small broadening of, at most, 20 nm at the blue side of the Soret band. Much larger differences between TPP and TEPP layers were found in the fluorescence spectra. The locations of the fluorescence maxima of the films are similar to those of the solutions, but in contrast to the equal fluorescence quantum yields in solution, films of TEPP exhibit

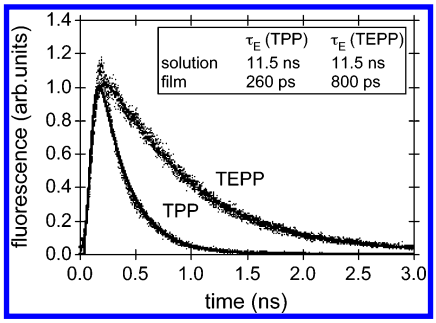

Figure 3. Fluorescence decay of 30 ± 5 nm thick TPP (solid line) and TEPP (dashed line) films on quartz together with the corresponding monoexponential fits. The exciton lifetimes in solution and in the films are given in the inset.

an approximately 20 times higher fluorescence quantum yield than TPP films. The fluorescence quantum yields of both films were found to be independent of the intensity of the excitation light. Hence, bimolecular exciton−exciton annihilation does not play a significant role at the intensities applied.

The solutions of TPP and TEPP were found to exhibit an identical fluorescence lifetime of 11.5 ns, which is comparable to literature values for TPP.[49,50] In contrast, the time-resolved fluorescence decays in Figure 3 show that excitons in TEPP films decay more slowly than those in TPP films. Fitting of a monoexponential decay convoluted over the excitation pulse duration and the time response of detection yields singlet exciton lifetimes equal to $\tau_E = 260$ ps and $\tau_E = 800$ ps for TPP and TEPP films, respectively. The exciton lifetime of 310 ps found by Hall and co-workers[51] for TPP films is comparable to the result from the current work.

The differences in fluorescence quantum yield and singlet exciton lifetime are caused by different rate constants for the exciton decay processes (Figure 1, processes 4−7). Since the porphyrin films are deposited on quartz, interfacial electron transfer can be ruled out. The possible decay pathways are intersystem crossing, radiationless decay, and fluorescence. The exciton lifetime is related to the rate constants for fluorescence (k_F), radiationless decay (k_{NR}), and intersystem crossing (k_{ISC}) by[52]

$$\tau_E = \frac{1}{k_F + k_{NR} + k_{ISC}} \quad (7)$$

The fluorescence quantum yield (ϕ_F) is given by[52]

$$\phi_F = \frac{k_F}{k_F + k_{NR} + k_{ISC}} = k_F \cdot \tau_E \quad (8)$$

Using the experimental exciton lifetimes and the ratio of the fluorescence quantum yields in TPP and TEPP films, it is found from eqs 7 and 8 that the fluorescence rate constant in TEPP is approximately 7 times higher than in TPP. For metal-free porphyrins, the time scale for intersystem crossing is on the order of 10 ns.[50] Since the exciton lifetimes are much shorter, the contribution of intersytem crossing (k_{ISC}) can be neglected in eqs 7 and 8. Hence, the combination of a longer τ_E and a higher k_F for TEPP films is only possible if k_{NR} is smaller than in TPP films. From the results described above, it can be deduced that k_{NR} for TEPP films is at least 3 times smaller than for TPP films; see Appendix A (Supporting Information).

Photoconductivity Measurements. *Microwave Conductivity Transients.* Figure 4 shows the TRMC signals obtained on pulsed illumination at 430 nm of a bare TPP film on quartz, a TPP/TiO_2 bilayer, and a TEPP/TiO_2 bilayer. The samples were

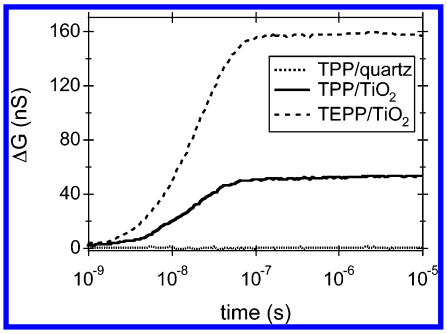

Figure 4. TRMC signals obtained on backside pulsed excitation at 430 nm ($5 \cdot 10^{12}$ photons/cm^2/pulse) of a bare TPP film (dotted line), a 42 ± 5 nm TPP/TiO_2 bilayer (solid line), and a 37 ± 5 nm TEPP/TiO_2 bilayer (dashed line).

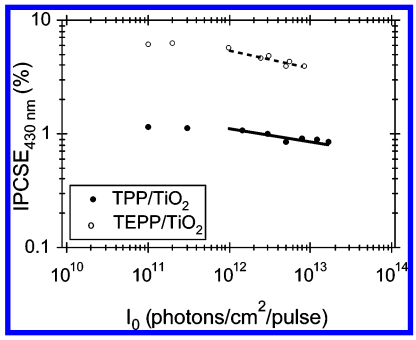

Figure 5. Intensity dependence of the IPCSE on 430 nm backside pulsed illumination of a 42 ± 5 nm TPP/TiO_2 bilayer (solid dots) and a 37 ± 5 nm TEPP/TiO_2 bilayer (open dots).

illuminated through the quartz substrate ("backside"), yielding a high initial exciton concentration near the porphyrin/TiO_2 interface for the bilayer systems. Since the mobility of holes in porphyrins is much lower than the mobility of electrons in TiO_2,[45,53] the observed change in photoconductivity is due to the production of mobile electrons in the TiO_2 film. The initial rise of the TRMC signals is due to the 18 ns instrument response time of the system.

As can be seen in Figure 4, illumination of a TPP film on quartz did not result in any detectable TRMC signal. The same was found for a TEPP film on quartz. Excitation of bare TiO_2 layers with visible light was found to result in a small short-lived signal, which is ascribed to sub-bandgap excitation (Figure 1, process 11) of electronic states within the optical band gap.[5] Hence, the large and long-lived photoconductance observed for the bilayer systems demonstrates the photosensitization of the anatase TiO_2 by the porphyrin layer. The charge-separated state persists to the microsecond domain. The eventual decay of the photoconductance is due to interfacial electron−hole recombination and/or electron trapping. Since the current experiments were carried out in the absence of charge-collecting electrodes, the decay of the photoconductance is not due to extraction of charge carriers. For the TEPP/TiO_2 bilayer, a significantly higher TRMC signal was found than for the TPP/TiO_2 bilayer, which can be attributed to more efficient charge separation in the TEPP/TiO_2 bilayer, as will be discussed below.

Charge Separation Efficiencies. As discussed in section 2.3, the IPCSE can be calculated from the TRMC signal obtained upon UV excitation of bare TiO_2 and the TRMC signal observed upon pulsed illumination of a bilayer with visible light, using eq 6. Figure 5 shows the IPCSE values determined on 430 nm excitation of the TPP/TiO_2 and TEPP/TiO_2 bilayers as a function of the incident light intensity. At intensities below 10^{12} photons/cm^2/pulse, the IPCSE values were found to be independent of the light intensity. Hence, exciton−exciton annihilation and

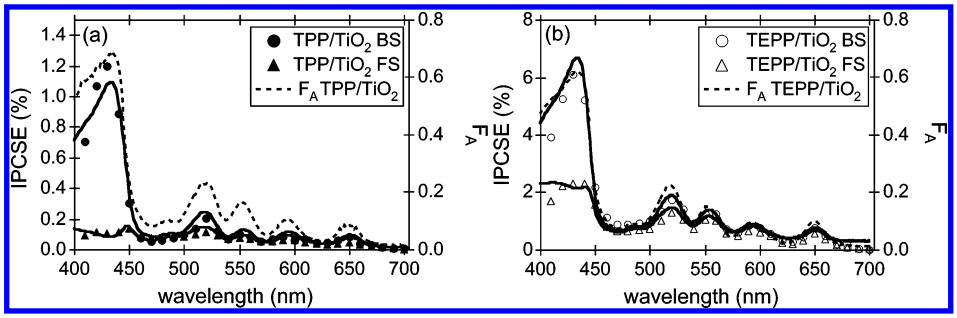

Figure 6. The fraction of absorbed light F_A (dashed line) and the experimental IPCSE values of a 42 ± 5 nm TPP/TiO_2 bilayer as a function of wavelength on backside (dots) and front-side (triangles) illumination and the wavelength dependence of the IPCSE calculated using eq 10 with $\phi_{inj} = 0.37$ and $\Lambda_E = 7$ Å (a) (solid lines). The results for a 37 ± 5 nm TEPP/TiO_2 bilayer are shown in (b), with $\phi_{inj} = 0.37$ and $\Lambda_E = 75$ Å.

bimolecular charge recombination processes can be neglected at these low intensities. At these intensities, the IPCSE of the TPP/TiO_2 bilayer amounts to 1.2%, in agreement with earlier studies,[54] and to 6.2% for the TEPP/TiO_2 bilayer.

For intensities larger than 10^{12} photons/cm^2 per pulse, the IPCSE was found to decrease with I_0 according to

$$\text{IPCSE} \propto {I_0}^{\delta-1} \tag{9}$$

The exponents were found to be $\delta = 0.91$ and $\delta = 0.83$ for the TPP/TiO_2 and the TEPP/TiO_2 bilayers, respectively. Note that eq 9 corresponds to a power law dependence of the photoconductance on the intensity ($\Delta G \propto {I_0}^{\delta}$).

Figure 6 shows the IPCSE as a function of wavelength ("photoaction spectrum") for both bilayers determined on backside and front-side illumination as well as their optical attenuation spectra. The average illumination intensity was equal to $6 \cdot 10^{12}$ photons/cm^2/pulse. To correct for bimolecular effects due to variations in illumination intensity over this wavelength range, the measured IPCSE values were extrapolated to an illumination intensity of $1 \cdot 10^{11}$ photons/cm^2/pulse using eq 9. It is obvious that the photoaction spectra for backside illumination of both TPP/TiO_2 and TEPP/TiO_2 closely follow the corresponding optical attenuation spectra, which again demonstrates the photosensitization of TiO_2 by the porphyrin layers. In the case of backside illumination, excitons are mainly created near the porphyrin/TiO_2 interface. In contrast, front-side illumination leads mainly to the formation of excitons near the porphyrin/gas interface and, especially in the case of a short optical absorption length, only a few excitons near the porphyrin/TiO_2 interface. Since the thickness of the porphyrin layer is expected to largely exceed the exciton diffusion length, only excitons created near the porphyrin/TiO_2 interface result in charge-separated states. Hence, front-side illumination results in lower IPCSE values than backside illumination.

Parameters Affecting the IPCSE. The exciton diffusion length and the interfacial electron injection yield can be obtained using the theoretical model for the IPCSE described previously.[55] The IPCSE depends on the fraction of incident photons that is reflected by the bilayer (F_R), the number of excitons that reaches the porphyrin/TiO_2 interface normalized to the number of incident photons (S), and the interfacial injection yield relative to all modes of interfacial exciton deactivation (ϕ_{inj})

$$\text{IPCSE} = (1 - F_R) \cdot S(\alpha, L, \Lambda_E) \cdot \phi_{inj} \cdot 100\% \tag{10}$$

S depends on the exponential optical absorption coefficient (α), the porphyrin layer thickness (L), and the exciton diffusion length (Λ_E). Analytical expressions for S on backside (S_{BQ}) and front-side illumination (S_{FQ}) have been derived by solving the classical diffusion equation for steady-state conditions, and they are given in Appendix B (Supporting Information).[55−57] Accurate values for ϕ_{inj} and Λ_E can be obtained by varying the thickness of the porphyrin layer. If the thickness of the porphyrin layer is much larger than the exciton diffusion length, a large difference in IPCSE between backside and front-side illumination can be expected. In that case, the IPCSE does not vary much with layer thickness for backside illumination. This is because mainly those excitons created within a distance Λ_E from the interface can undergo interfacial charge separation. In contrast, for front-side illumination, increasing L leads to a smaller concentration of excitons near the porphyrin/TiO_2 interface. As a consequence, the IPCSE decreases with increasing L and eventually becomes zero. If the thickness of the porphyrin layer is smaller than the exciton diffusion length, the difference in IPCSE between backside and front-side illumination disappears, since in this case, all excitons are able to reach the porphyrin/TiO_2 interface. Increasing L will then lead to an increase of the IPCSE, since more light is absorbed as the layer becomes thicker.

Figure 7a,b shows the dependence of the IPCSE on the porphyrin layer thickness on backside and front-side illumination for TPP/TiO_2 and TEPP/TiO_2 bilayers, respectively. Since F_R varied between different samples, the ratio of IPCSE to $(1 - F_R)$ is shown. The data presented in Figure 7a exhibit a dependence of the IPCSE on L that does not agree with the expectations as discussed in the previous paragraph. This is most likely due to variation of porphyrin layer structure and consequently the exciton diffusion length, with the layer thickness, as will be discussed in the next section. The data in Figure 7b can be excellently described by eq 10 and eqs B1 and B2 in the Supporting Information (see Appendix B). Fits of these equations to the experimental data yield an exciton diffusion length of 75 Å and an interfacial electron injection yield $\phi_{inj} = 0.37$ for a TEPP/TiO_2 bilayer. With these parameters and the known wavelength dependence of α, the front-side and backside photoaction spectra for the TEPP/TiO_2 bilayer were also calculated; see Figure 6b. The calculated action spectra agree very well with the experimental results.

Although the thickness dependence of the IPCSE for the TPP/TiO_2 bilayers in Figure 7a cannot be described by eq 10 and eqs B1 and B2, the photoaction spectrum for a particular porphyrin layer thickness could be described by these equations; see the fits in Figure 6a. The photoaction spectrum in Figure 6a was obtained for a sample for which $L \gg \Lambda_E$. In this case, the IPCSE is mainly determined by the product of ϕ_{inj} and Λ_E. Therefore, it is not possible to determine accurate values of these parameters independently. Taking the interfacial electron injection yield in TPP/TiO_2 bilayers equal to those found for TEPP/TiO_2 layers yields an exciton diffusion length of 7 Å, which is more than 10 times smaller than Λ_E in TEPP layers.

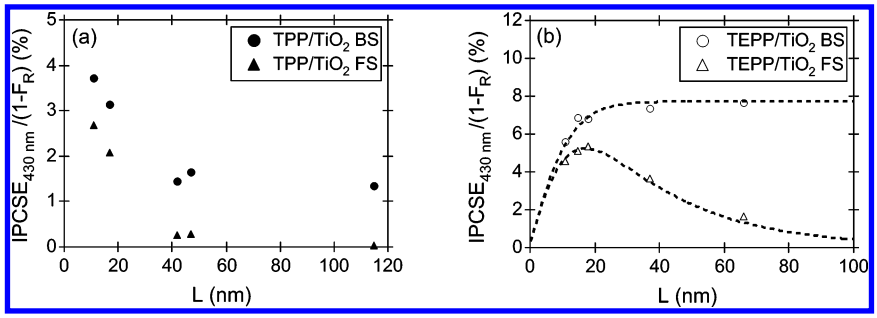

Figure 7. IPCSE/(1 − F_R) as a function of the porphyrin layer thickness for TPP/TiO_2 (a) and TEPP/TiO_2 (b) bilayers, obtained upon excitation at 430 nm with $5 \cdot 10^{12}$ photons/cm^2/pulse. Dots represent backside illumination, triangles front-side illumination.

Discussion

The exciton diffusion lengths and lifetimes can be used to determine the singlet exciton diffusion coefficient using eq 1. This yields a value of $2 \cdot 10^{-9}$ m^2/s for a TPP layer and a much higher value of $7 \cdot 10^{-8}$ m^2/s for a TEPP layer. Both values are much larger than the triplet exciton diffusion coefficient observed in Pd-substituted porphyrin layers ($8 \cdot 10^{-11}$ m^2/s).[38,39] For the porphyrin molecules considered here, exciton diffusion is expected to occur via the Förster mechanism.[58,59] Förster energy transfer occurs by the exchange of a virtual photon, with hopping rate k_{ET}, and can only occur if there is a nonzero overlap of the emission and the absorption spectra. The data in Figure 2b show that the latter condition is fulfilled. The exciton diffusion constant is linearly proportional to the fluorescence rate constant according to[58,60]

$$D_E = k_{ET} \cdot R_{DA}^2 = \frac{9000(\ln 10)\kappa^2 J_F k_F}{128\pi^5 n^4 N_A R_{DA}^4} \qquad (11)$$

In eq 11, κ^2 is a factor describing the relative orientation of the transition dipoles of donor and acceptor species, J_F an integral taking into account the overlap of the absorption and emission spectra, n the refractive index, N_A Avogadro's number, and R_{DA} the distance between donor and acceptor species. According to eq 11, the larger k_F found for TEPP layers leads to a higher exciton diffusion coefficient. The value of k_F for TEPP is 7 times higher than for TPP, while the exciton diffusion coefficient is a factor of 35 higher. This could also be because κ^2 and/or R_{DA} are different for TPP and TEPP layers.

The lower fluorescence rate constant found for TPP films could be caused by the presence of face-to-face molecular dimers or larger aggregates. In such aggregates, electronic coupling between the molecular orbitals on the individual molecules leads to a splitting of the electronic levels, as shown in Figure 8 for a dimer. In porphyrin molecules, the transition dipole moments for the S_0-S_2 and S_0-S_1 transitions are parallel to the plane of the molecule.[48] Hence, face-to-face molecular stacking leads to formation of H-aggregates.[61] For H-dimers, the in-phase interaction of the two transition dipole moments leads to the higher-lying E'' level, and the out-of-phase interaction yields the lower-lying E' level, as discussed by Kasha.[62] The optical transition between the E' exciton state and the ground state is forbidden. Analogously, in larger H-aggregates, the optical transition between the lowest exciton state and the ground state is forbidden. Hence, fluorescence from the lowest excited state is prevented by formation of H-aggregates. In that case, exciton diffusion between different H-aggregates via the Förster mechanism is impossible. The low fluorescence rate constant and the small exciton diffusion coefficient in TPP layers could thus be due to the presence of

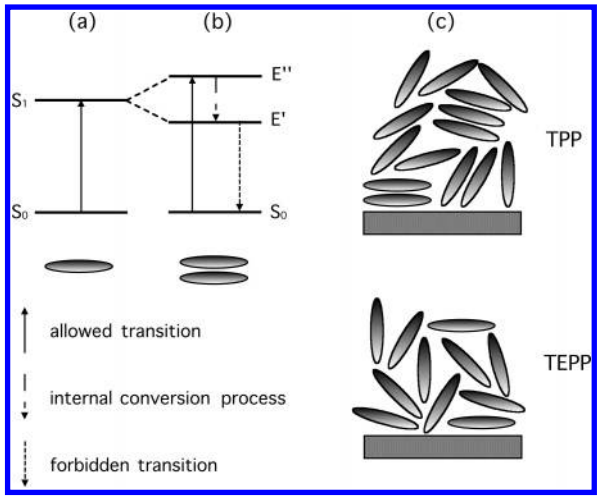

Figure 8. Representation of the energy levels of a porphyrin monomer (a) and a dimeric H-aggregate (b). In (c), a schematic view of the structure of TPP and TEPP layers is shown.

H-aggregates. The ethyl groups in TEPP seem to reduce the extent to which H-aggregates are present in the film. The stronger tendency of TPP molecules to form H-aggregates may be caused by the lower solubility in $CHCl_3$ due to the absence of alkyl side chains. The average distance or the relative orientation between individual molecules in nonaggregated domains in a film may differ from the mutual arrangement of different H-aggregates. These differences in R_{DA} or κ^2 may also lower D_E as follows from eq 11, explaining that the exciton diffusion coefficient in TEPP layers is 35 times larger than in TPP layers, while the value of k_F is only a factor of 7 higher.

The tendency of TPP molecules to form H-aggregates can also explain the unexpected thickness dependence of the IPCSE for TPP/TiO_2 bilayers, shown in Figure 7a. Thicker TPP layers were prepared by spin-coating from a more concentrated solution, in which the formation of H-aggregates is expected to occur to a larger extent. If this is the case, the exciton diffusion length decreases for thicker TPP layers. This would in turn lead to a decrease of the IPCSE with increasing porphyrin layer thickness, as indeed is observed for TPP (see Figure 7a). Since the shapes of the fluorescence spectra of the TPP and TEPP layers (Figure 2b) are very similar, it is likely that the remaining fluorescence of the TPP layer is due to nonaggregated porphyrin molecules. This indicates the presence of both H-aggregates and single molecules in TPP layers.

Note that the formation of H-aggregates in a film does not necessarily lead to a blue shift of the absorption spectrum as compared to the solution spectrum. This can be because the change in dielectric environment upon going from a solution to a film may result in a red shift, which can dominate over the blue shift due to formation of H-aggregates. The identical onset

of the Soret band at the red side observed for TPP and TEPP films indicates that in both films nonaggregated molecules are present. The tail at the blue side of the Soret band observed for TPP films is attributed to a minor amount of H-aggregates.

Since the energy of an exciton on an H-aggregate will be lower than on an individual molecule in a less ordered domain in the film, H-aggregates may act as exciton traps. Exciton diffusion between H-aggregates is hampered because of the negligible Förster transfer rate, as a result of the forbidden fluorescence transition. However, excitons may well be delocalized over an entire H-aggregate.[63] Hence, in case the dye layer consists of H-aggregates oriented perpendicularly to the TiO_2 substrate and in contact with the latter, the exciton diffusion length corresponds to the length of the H-aggregate. In case long H-aggregates can be arranged in this manner, a high charge separation efficiency may be achieved. Our work, however, indicates that a relatively long exciton diffusion length and consequently a high charge separation efficiency can also be realized in a layer in which energy transfer occurs between randomly oriented single molecules.

The value of $\phi_{inj} = 0.37$ found for the interfacial electron injection yield in a TEPP/TiO_2 bilayer is significantly smaller than the electron injection yield close to unity reported earlier for *meso*-tetra(4-carboxyphenyl)porphyrin on nanocrystalline TiO_2.[64] Note that ϕ_{inj} is defined as the fractional yield of free electrons due to dissociation of excitons that have reached the interface between the porphyrin layer and the TiO_2. Hence, the interfacial injection yield is not affected by the exciton diffusion length, and therefore, the present value of ϕ_{inj} can be directly compared with the results for the system studied in ref 64 in which each porphyrin molecule is directly attached to TiO_2. The fact that the electron injection yield found in the present work differs from that in ref 64 could be because the measurements described in ref 64 were carried out in the presence of an external electric field, which prevents geminate recombination. Alternatively, it could be argued that the absence of an anchoring group reduces the electronic interaction between the porphyrin molecule and TiO_2, thus leading to a lower electron injection yield.[20] Enhancement of the relatively low injection yield offers the opportunity of a further improvement of the charge separation efficiency in TEPP/TiO_2 bilayer systems.

Conclusions

The charge separation efficiency per incident photon in TEPP/TiO_2 bilayers is 6.2% for excitation at the Soret band maximum, which is considerably higher than the efficiency of 1.2% found for TPP/TiO_2 bilayers. This difference is attributed to a larger exciton diffusion length in TEPP. The exciton diffusion length in TEPP is found to be 75 Å, while this is only 7 Å in TPP layers. The larger exciton diffusion length in TEPP layers is mainly due to a higher exciton diffusion coefficient, which is equal to $7 \cdot 10^{-8}$ m^2/s for TEPP and only $2 \cdot 10^{-9}$ m^2/s for TPP. The larger exciton diffusion length is also caused by a longer exciton lifetime, which is found to be 800 ps for TEPP and only 260 ps for TPP. The lower exciton diffusion constant in TPP layers is explained in terms of the presence of H-aggregates.

Acknowledgment. The authors thank Dr. F. C. Grozema, Dr. H. Donker, and Dr. J. M. Warman for fruitful discussions. The research was supported financially by the Delft Research Centre for Sustainable Energy.

Supporting Information Available: Appendixes A and B. This material is available free of charge via the Internet at http://pubs.acs.org.

References and Notes

(1) Grätzel, M. *Nature (London)* **2001**, *414*, 338.
(2) Savenije, T. J.; Warman, J. M.; Goossens, A. *Chem. Phys. Lett.* **1998**, *287*, 148.
(3) Breeze, A. J.; Schlesinger, Z.; Carter, S. A.; Brock, P. J. *Phys. Rev. B* **2001**, *6412*, 125205.
(4) Kerp, H. R.; Donker, H.; Koehorst, R. B. M.; Schaafsma, T. J.; van Faassen, E. E. *Chem. Phys. Lett.* **1998**, *298*, 302.
(5) Kroeze, J. E.; Savenije, T. J.; Warman, J. M. *J. Photochem. Photobiol., A* **2002**, *148*, 49.
(6) O'Regan, B.; Grätzel, M. *Nature (London)* **1991**, *353*, 737.
(7) Bach, U.; Lupo, D.; Comte, P.; Moser, J. E.; Weissortel, F.; Salbeck, J.; Spreitzer, H.; Grätzel, M. *Nature (London)* **1998**, *395*, 583.
(8) Sommeling, P. M.; Spath, M.; Smit, H. J. P.; Bakker, N. J.; Kroon, J. M. *J. Photochem. Photobiol., A* **2004**, *164*, 137.
(9) Kruger, J.; Plass, R.; Grätzel, M. *Appl. Phys. Lett.* **2002**, *81*, 367.
(10) Schmidt-Mende, L.; Zakeeruddin, S. M.; Grätzel, M. *Appl. Phys. Lett.* **2005**, *86*, 013504.
(11) Beek, W. J. E.; Wienk, M. M.; Janssen, R. A. J. *Adv. Mater.* **2004**, *16*, 1009.
(12) Kay, A.; Humphrybaker, R.; Grätzel, M. *J. Phys. Chem.* **1994**, *98*, 952.
(13) Fessenden, R. W.; Kamat, P. V. *J. Phys. Chem.* **1995**, *99*, 12902.
(14) Boschloo, G. K.; Goossens, A. *J. Phys. Chem.* **1996**, *100*, 19489.
(15) Koehorst, R. B. M.; Boschloo, G. K.; Savenije, T. J.; Goossens, A.; Schaafsma, T. J. *J. Phys. Chem. B* **2000**, *104*, 2371.
(16) Tachibana, Y.; Haque, S. A.; Mercer, I. P.; Durrant, J. R.; Klug, D. R. *J. Phys. Chem. B* **2000**, *104*, 1198.
(17) Kroeze, J. E.; Savenije, T. J.; Warman, J. M. *J. Am. Chem. Soc.* **2004**, *126*, 7608.
(18) Hasobe, T.; Kashiwagi, Y.; Absalom, M. A.; Sly, J.; Hosomizu, K.; Crossley, M. J.; Imahori, H.; Kamat, P. V.; Fukuzumi, S. *Adv. Mater.* **2004**, *16*, 975.
(19) Ma, T. L.; Inoue, K.; Yao, K.; Noma, H.; Shuji, T.; Abe, E.; Yu, J. H.; Wang, X. S.; Zhang, B. W. *J. Electroanal. Chem.* **2002**, *537*, 31.
(20) Ma, T. L.; Inoue, K.; Noma, H.; Yao, K.; Abe, E. *J. Photochem. Photobiol., A* **2002**, *152*, 207.
(21) Odobel, F.; Blart, E.; Lagree, M.; Villieras, M.; Boujtita, H.; El Murr, N.; Caramori, S.; Bignozzi, C. A. *J. Mater. Chem.* **2003**, *13*, 502.
(22) Clifford, J. N.; Yahioglu, G.; Milgrom, L. R.; Durrant, J. R. *Chem. Commun.* **2002**, 1260.
(23) Wamser, C. C.; Kim, H. S.; Lee, J. K. *Opt. Mater.* **2003**, *21*, 221.
(24) Campbell, W. M.; Burrell, A. K.; Officer, D. L.; Jolley, K. W. *Coord. Chem. Rev.* **2004**, *248*, 1363.
(25) Kroeze, J. E.; Koehorst, R. B. M.; Savenije, T. J. *Adv. Funct. Mater.* **2004**, *14*, 992.
(26) Gregg, B. A. *Mol. Cryst. Liq. Cryst. Sci. Technol., Sect. A* **1994**, *257*, 219.
(27) Balaban, T. S.; Bhise, A. D.; Fischer, M.; Linke-Schaetzel, M.; Roussel, C.; Vanthuyne, N. *Angew. Chem., Int. Ed.* **2003**, *42*, 2140.
(28) Balaban, T. S.; Linke-Schaetzel, M.; Bhise, A. D.; Vanthuyne, N.; Roussel, C.; Anson, C. E.; Buth, G.; Eichhofer, A.; Foster, K.; Garab, G.; Gliemann, H.; Hoddard, R.; Javorfi, T.; Powell, A. K.; Rosner, H.; Schimmel, T. *Chem. Eur. J.* **2005**, *11*, 2268.
(29) Savenije, T. J.; Koehorst, R. B. M.; Schaafsma, T. J. *J. Phys. Chem. B* **1997**, *101*, 720.
(30) Savenije, T. J.; Goossens, A. *Phys. Rev. B* **2001**, *6411*.
(31) Kroon, J. M.; Koehorst, R. B. M.; vanDijk, M.; Sanders, G. M.; Sudholter, E. J. R. *J. Mater. Chem.* **1997**, *7*, 615.
(32) Maiti, N. C.; Mazumdar, S.; Periasamy, N. *J. Porphyr. Phthalocyanines* **1998**, *2*, 369.
(33) Khairutdinov, R. F.; Serpone, N. *J. Phys. Chem. B* **1999**, *103*, 761.
(34) Yatskou, N. N.; Apanasovich, V. V. *J. Appl. Spectrosc.* **2002**, *69*, 82.
(35) Leray, I.; Vernieres, M. C.; Pansu, R.; BiedCharreton, C.; Faure, J. *Thin Solid Films* **1997**, *303*, 295.
(36) Yatskou, N. N.; Apanasovich, V. V.; Koehorst, R. B. M.; Hoek, A. v.; Schaafsma, T. *J. Appl. Spectrosc.* **2003**, *70*, 372.
(37) Anderson, N. A.; Ai, X.; Lian, T. Q. *J. Phys. Chem. B* **2003**, *107*, 14414.
(38) Kroeze, J. E.; Savenije, T. J.; Warman, J. M. *Adv. Mater.* **2002**, *14*, 1760.
(39) Kroeze, J. E.; Savenije, T. J.; Candeias, L. P.; Warman, J. M.; Siebbeles, L. D. A. *Sol. Energy Mater. Sol. Cells* **2005**, *85*, 189.
(40) Scurlock, R. D.; Wang, B.; Ogilby, P. R.; Sheats, J. R.; Clough, R. L. *J. Am. Chem. Soc.* **1995**, *117*, 10194.
(41) Granzhan, A.; Penzkofer, A.; Hauska, G. *J. Photochem. Photobiol., A* **2004**, *165*, 75.
(42) Van de Krol, R.; Goossens, A.; Schoonman, J. *J. Electrochem. Soc.* **1998**, *145*, 3697.
(43) De Haas, M. P.; Warman, J. M. *Chem. Phys.* **1982**, *73*, 35.

(44) Savenije, T. J.; De Haas, M. P.; Warman, J. M. *Z. Phys. Chem. (Muenchen, Ger.)* **1999**, *212*, 201.
(45) Bak, T.; Nowotny, J.; Rekas, M.; Sorrell, C. C. *J. Phys. Chem. Solids* **2003**, *64*, 1069.
(46) Shiga, A.; Tsujiko, A.; Yae, S.; Nakato, Y. *Bull. Chem. Soc. Jpn.* **1998**, *71*, 2119.
(47) Schouten, P. G.; Warman, J. M.; De Haas, M. P.; Fox, M. A.; Pan, H. L. *Nature (London)* **1991**, *353*, 736.
(48) Gouterman, M. *The Porphyrins*; Academic Press: New York, 1978; Vol. 3.
(49) Levanon, H.; Vega, S. *J. Chem. Phys.* **1974**, *61*, 2265.
(50) Kalyanasundaram, K.; Neumann-Spallart, M. *J. Phys. Chem.* **1982**, *86*, 5163.
(51) Hall, R. S.; Oh, Y. S.; Johnson, C. S. *J. Phys. Chem.* **1980**, *84*, 756.
(52) Turro, N. J. *Modern Molecular Photochemistry*; The Benjamin/Cummings Publishing Company, Inc.: Menlo Park, CA, 1978.
(53) Checcoli, P.; Conte, G.; Salvatori, S.; Paolesse, R.; Bolognesi, A.; Berliocchi, A.; Brunetti, F.; D'Amico, A.; Di Carlo, A.; Lugli, P. *Synth. Met.* **2003**, *138*, 261.
(54) Kroeze, J. E.; Savenije, T. J.; Warman, J. M. *Proc. SPIE* **2003**, *4801*, 67.
(55) Kroeze, J. E.; Savenije, T. J.; Vermeulen, M. J. W.; Warman, J. M. *J. Phys. Chem. B* **2003**, *107*, 7696.
(56) Simpson, O. *Proc. R. Soc. London, Ser. A* **1957**, *238*, 402.
(57) Sodergren, S.; Hagfeldt, A.; Olsson, J.; Lindquist, S. E. *J. Phys. Chem.* **1994**, *98*, 5552.
(58) Förster, T. H. *Discuss. Faraday Soc.* **1959**, *27*, 7.
(59) Faure, S.; Stern, C.; Guilard, R.; Harvey, P. D. *J. Am. Chem. Soc.* **2004**, *126*, 1253.
(60) Sariciftci, N. S. *Prog. Quantum Electron.* **1995**, *19*, 131.
(61) May, V.; Kühn, O. *Charge and Energy Transfer Dynamics in Molecular Systems. A Theoretical Introduction*; Wiley-VCH: Berlin, 2000.
(62) Kasha, M.; Rawls, H. R.; Ashraf Et.-Bayoumi, M. *Pure Appl. Chem.* **1965**, *11*, 371.
(63) Markovitsi, D.; Gallos, L. K.; Lemaistre, J. P.; Argyrakis, P. *Chem. Phys.* **2001**, *269*, 147.
(64) Cherian, S.; Wamser, C. C. *J. Phys. Chem. B* **2000**, *104*, 3624.